Nanoscale

PAPER

Cite this: DOI: 10.1039/d4nr00978a

Characterisation of the morphology of surface-assembled Au nanoclusters on amorphous carbon

Malcolm Dearg, [a,b] Sean Lethbridge, [c] James McCormack,[c] Richard E. Palmer *[c] and Thomas J. A. Slater *[a]

Received 7th March 2024,
Accepted 13th May 2024

DOI: 10.1039/d4nr00978a

rsc.li/nanoscale

In this study, aberration-corrected scanning transmission electron microscopy is employed to investigate the morphology of Au clusters formed from the aggregation of single atoms sputtered onto an amorphous carbon surface. The morphologies of surface-assembled clusters of $N > 100$ atoms are referenced against the morphologies of size-selected clusters determined from previously published results. We observe that surface-assembled clusters (at the conditions employed here) are approximately spherical in shape. The structural isomers of the imaged clusters have also been identified, and the distribution of structural types is broadly in agreement with those from size-selected cluster deposition sources. For clusters of approximately 147 atoms, we find a preference for icosahedra over decahedra and truncated octahedra, but at this size there is a high proportion of unidentified/amorphous structures. At around 309 atoms, we find a preference for decahedra over icosahedra and truncated octahedra, but over half the structures remain unidentifiable/amorphous. For sizes above approximately 561 atoms we are able to identify most of the structures, and find decahedra are still the most favoured, although in competition with single-crystal fcc morphologies. The similarity in structure between surface-assembled and size-selected clusters from a cluster source provides evidence of the relevance of size-selected cluster studies to clusters synthesised by other, industrially relevant, methodologies.

The size and structure of metal nanoclusters is crucially important to both their catalytic activity and selectivity in a wide array of reactions.[4,5] Their size inherently regulates the surface area to volume ratio of the catalyst, with single atom catalysts maximising availability of metal atoms.[6] The cluster structure determines the coordination of surface atoms and thus the sites available for adsorption and desorption of molecular species.[7]

In this study, we investigate the morphology of Au clusters formed by surface-assembly of atoms sputtered onto an amorphous carbon film using aberration-corrected high-angle annular dark field scanning transmission electron microscopy (HAADF-STEM). In particular, we aim to understand how the structures of surface-assembled clusters compare with those produced by size-selected cluster beam deposition. Clusters deposited from cluster beam (*e.g.* gas-condensation) sources are often used for exemplar studies of metal clusters in catalysis. Understanding the differences in morphology between clusters produced *via* surface growth, *versus* those from cluster sources, is therefore important. This is particularly so because the process to form surface-assembled clusters is representative of those employed in the majority of commercial heterogeneous catalysts, *i.e.* is similar to the surface growth of nanoclusters during calcination and reduction of metal precursors. Specifically, we aim to understand whether clusters from gas-condensation sources are representative of surface-assembled clusters.

Gold nanoclusters are of particular interest, because of their excellent catalytic activity in a number of reactions[8] and the small energy differences between different structural isomers that results in competition between different structures at small cluster sizes.[9,10] Gold nanoclusters typically assume one of three structures: Icosahedral (Ih), Decahedral (Dh) and single-crystal fcc (fcc),[9,10] which determine the surface sites available for catalysis. In this study, we aim to quantify the proportion of each structural isomer in a size range between 100 and 1000 atoms for surface-assembled clusters.

Due to the formation process of surface-assembly, we expect to find populations of cluster structures that represent equilibrium structure distributions (assuming a weak cluster-surface interaction). If correct, we expect the distribution of isomer populations to be broadly comparable to those found

[a]*Cardiff Catalysis Institute, School of Chemistry, Cardiff University, Cardiff, CF24 4HQ, UK. E-mail: SlaterT2@cardiff.ac.uk; Tel: +44 (0)29 2087 9966*
[b]*School of Physics, Engineering and Technology, University of York, York, YO10 5DD, UK*
[c]*Nanomaterials Lab, Department of Mechanical Engineering, Faculty of Science and Engineering, Swansea University, Bay Campus, Swansea, SA1 8EN, UK*

in clusters formed *via* gas-condensation with long condensation lengths,[11] or those that have been annealed.[12] This is in contrast to metastable structures that can be formed *via* short condensation lengths *via* gas-condensation.[11]

In the present study, we find that clusters formed from atomic sputtering and surface-assembly (at the particular conditions used here) have a near-spherical morphology, similar to those from gas-condensation cluster sources. Further, we find the distribution of non-amorphous isomers is dominated by icosahedral structures for clusters of less than approximately 436 atoms, while above this size decahedral and fcc structures dominate. The distribution of structural isomers found at the larger sizes are in broad agreement with previous studies on equilibrium distributions from gas-condensation cluster sources.

1. Investigation of sphericity

Two methodologies are employed to determine the sphericity of Au clusters surface-assembled from sputtered atoms on an amorphous carbon film. Firstly, the number of atoms in a population of surface-assembled clusters is determined *via* HAADF-STEM intensity (calibrated through comparison to size-selected clusters known to be quasi-spherical). Comparison of the number of atoms in each cluster to its diameter/radius provides evidence of sphericity *versus* hemisphericity.

Fig. 1 shows a comparison of surface-assembled cluster diameters (red data points) against those of size-selected clusters (blue data points). Lines are plotted for expected diameter *versus* number of atoms for spherical and hemispherical particles. The equations for diameter *versus* number of atoms for nanoparticles can be derived from the volume of a sphere:

$$V_s = 4/3\pi {r_s}^3, \quad (1)$$

where V_s is the volume of a sphere, and r_s is the spherical radius. Taking the volume of the unit cell of bulk Au, $V = a^3$, in which there are 4 Au atoms, where a is the lattice parameter of Au, we can define a sphere of radius r_s to have the following number of atoms:

$$N = 4(4/3)\pi r^3/a^3, \quad (2)$$

which can be rearranged to give the approximate diameter of spherical and hemispherical nanoparticles with a number of atoms N, as follows:

$$D_s = \kappa N^{1/3}, \quad (3)$$

for spherical clusters, and for hemispherical clusters:

$$D_h = \kappa(2N)^{1/3}, \quad (4)$$

where D_s is the spherical diameter, D_h is the hemispherical diameter and κ represents approximately 0.8 multiplied by the Au lattice parameter (0.408 nm).

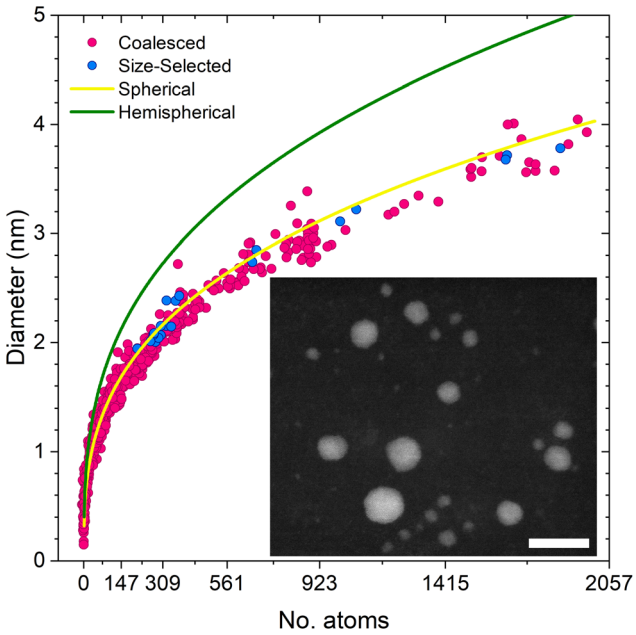

Fig. 1 Plot of the equivalent circular diameter of clusters for a given number of atoms. The green line represents the hemispherical distribution of diameters (eqn (4)), while the spherical (eqn (3)) is represented by the yellow line. Red data points are surface-assembled clusters and blue data points are size-selected clusters, which are known to be quasi-spherical. Inset is an example HAADF-STEM image of surface-assembled Au clusters on a carbon support, taken normal to the carbon surface, showing clusters to have a near-circular profile across a range of sizes. Inset scale bar of 10 nm.

The number of atoms can be directly obtained from the summed HAADF-STEM intensity associated with each cluster, due to the fact that the intensity scales linearly with number of atoms (up to a certain sample thickness).[13] Calibration of HAADF-STEM intensity to number of atoms is performed through imaging of size-selected clusters of a known number of atoms (309 ± 9 atoms), which are also known to be approximately spherical. As the imaging of both size-selected and surface-assembled clusters were performed under identical conditions and essentially within the same time window,‡ the calibration is applicable to the images of surface assembled-clusters. The errors on the number of atoms within size-selected clusters (approximately 2%) and the drift in emission current (2%) combine to give an approximate error of 3% on the size of measured clusters, which should be taken as the error on all measurements of size of surface-grown clusters. The calibrated number of atoms *versus* diameter clearly illustrates that the surface-assembled clusters across the entire

‡Both the surface-assembled and the size selected clusters were measured in a JEOL ARM300F at 300 kV under the same microscope alignment conditions and within 1 hour of each other to minimise any temporal drifts in the measurement system. The amplifier gain and amplitude/offset were maintained between all images. The emission current drift between size-selected and surface-assembled samples is of the order of 2%.

range of sizes from 100 atoms to almost 2000 are approximately quasi-spherical.

A confirmation of cluster sphericity is provided through imaging the sample tilted to a high angle with respect to the electron beam. By tilting the sample it is possible to directly inspect the angle of interaction of the cluster with the support to see if any wetting-like behaviour is occurring, or if there is any flattening of the sphere with respect to the support. Tilting clusters through ±70°, the vast majority of clusters maintain a circular projected cross-section, Fig. 2e, indicating that they are quasi-spherical. We support these observations with comparison against simulations of hemispherical clusters, Fig. 2a–d. The simulated projection of hemispherical cluster geometries at an angle of ±70° reveal a clear change in their projected outline, with a shrinking in projected diameter perpendicular to the tilt axis. We do not observe this change in projected diameter in clusters below 1000 atoms in size in the experimental images.

Through the two different methodologies outlined, we have determined that clusters below 1000 atoms in size, surface-assembled from sputtered single atoms, are close to spherical in morphology. This observation contrasts with previous findings of a wider distribution of morphologies[14] (N. P. Young *et al.*, 2008), which found many near-hemispherical clusters of surface-assembled atoms produced by thermal evaporation on the same type of amorphous carbon support. We postulate that the difference may be due to different deposition rates in the sputtering employed here in comparison to the thermal evaporation employed by Young *et al.* The sputtering flux in the samples in this study is comparatively low and therefore the cluster atoms are more likely to have time to arrange into a low-energy state. It may be a feature of atoms depositing at higher flux that there is a wider distribution in morphology, including hemispherical clusters which may be metastable, *i.e.* kinetically "trapped" before being able to relax to a lower energy. Additionally, the spherical clusters found here on carbon are in contrast to the 2D and hemispherical structures regularly observed on thin oxide films,[15] demonstrating the importance of the interaction between Au and the support material.

2. Investigation of structural isomer distribution

In this section we determine the proportion of surface-assembled clusters belonging to each structural isomer (icosahedral, decahedral, fcc and unidentified/amorphous). Fig. 3 shows the distribution of classified structural isomers for clusters surface-assembled from Au atoms sputtered onto amorphous carbon films, for ranges of atom numbers centred around magic numbers. The results from Fig. 3 are summarised in Table 1.

The structural isomers of clusters have been identified using the Simulation Atlas method,[2,16] which provides an extensive set ('Atlas') of HAADF-STEM images of idealised clusters. Not all clusters could be identified as one of the three structural isomers; this can be for a variety of reasons such as: image quality, cluster motion under the beam, or genuinely amorphous/glassy structures.

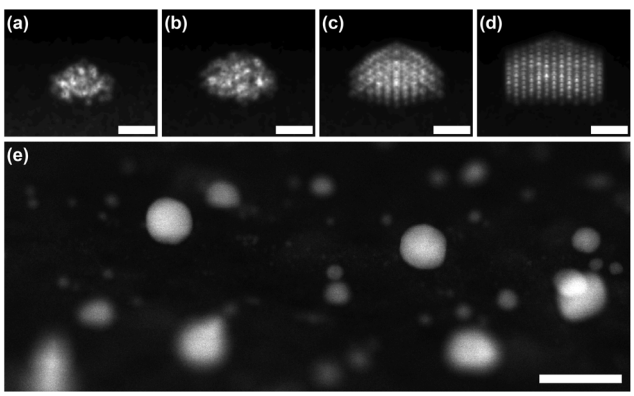

Fig. 2 Comparison of HAADF-STEM simulations of hemi-spherical truncated clusters on carbon at −70° to experimental data. (a) −70° projection of amorphised hemi-spherical Au147 icosahedron. (b) −70° projection of amorphised hemi-spherical Au309 decahedron. (c) −70° projection of hemi-spherical Au509 decahedron. (d) −70° projection of hemi-spherical Au923 truncated octahedron. (e) Wide field-of-view experimental HAADF-STEM image acquired at −70° showing all clusters under 1000 atoms in size are approximately spherical. (a–d) Scale bar of 1 nm. (e) Scale bar of 20 nm.

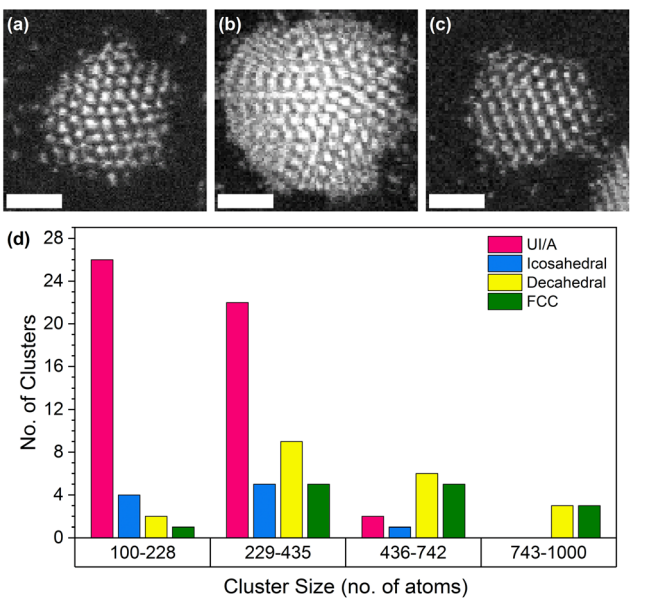

Fig. 3 (a–c) Experimental images of surface-grown clusters showing clear examples of decahedral (a), icosahedral (b) and truncated fcc (c) morphologies. Scale bars of 1 nm. (d) Summary of isomer distributions for surface-assembled clusters. Bin ranges for the cluster sizes are nominally centred around the "magic numbers" of 147, 309, 561 and 923. Cluster identification was performed through manual comparison of structural motifs to a Simulation Atlas of clusters of different sizes and orientations.

Table 1 Literature comparison of our findings

	Isomer			
Cluster size (atoms)	Ih	Dh	FCC	UI/A
100–228	12%	6%	3%	79%
229–435	12%	22%	12%	54%
436–742	7%	43%	36%	14%
743–1000	0%	50%	50%	0%
Li 2008[13]				
Size	Ih	Dh	FCC	UI/A
309	8%	32%	25%	35%
Wells 2015[1]				
Size	Ih	Dh	FCC	UI/A
561	2%	43%	36%	19%
742	3%	46%	37%	14%
923	4%	41%	31%	24%
	Au923			
Wang 2012[2] Irradiation time	Ih	Dh	FCC	UI/A
0	53.16%	22.78%	24.05%	—
>160	1.27%	60.75%	37.97%	—
	Au561			
Foster 2018[3] Temperature	Ih	Dh	FCC	UI/A
20 °C	3%	32%	39%	26%

Comparison of classification results of our work against those of Wells (2015)[1], Wang (2012)[2] and Foster (2018)[3]. Clusters are classified as face-centred-cubic (FCC), decahedron (Dh), icosahedron (Ih) or unidentified/amorphous (UI/A).

Our results show that unidentified/amorphous structures dominate the lower size range of clusters, from 100–435 atoms, with the proportion of unidentified/amorphous clusters rapidly decreasing in the range 436–742 atoms. The reduction in the proportion of unidentified/amorphous clusters with increasing size could be due to electron beam interactions, smaller clusters may be more influenced by the electron beam and thus more likely to move/rotate. However, smaller clusters may also show a preference for amorphous/glassy structures without the influence of the electron beam.[17–19] Clusters in the size range 436–1000 atoms are predominantly fcc (approximately 40%) or decahedral (approximately 45%). There is also a relatively high abundance of icosahedra at lower sizes (12%), which decreases at larger sizes.

Table 1 compares the results obtained here to results from studies of size-selected clusters in previously published literature.[1–3,11]

Our results cover a broad range of sizes and do not overlap with previously published experimental data until a size of 309 atoms. Comparing our data to that corresponding to clusters of 309 atoms from a previous study,[13] the clear difference is a lower proportion of identifiable/crystalline clusters in comparison to the present study. The relative proportions of crystalline isomers (ignoring unidentified/amorphous clusters) are similar to those in the range 229–435 found here, although the present study has fewer icosahedra and more fcc structures than the proportions determined for size-selected clusters. We see a similar degree of unidentified/amorphous classifications between 436–742 in our data compared with the reported 561 and 742 results of Wells *et al.*,[1] and the 561 results of Foster *et al.*[3] However, Wells *et al.*[1] report about a quarter of their clusters around 923 to be amorphous still, while for our surface-assembled clusters we find no amorphous clusters above 742 atoms. This is likely due to the "templated growth" of the clusters studied by Wells *et al.*, where observations indicated isomer distributions were maintained through different size ranges due to templated growth over an initial smaller core. Differences in our observations could also be due to differences in microscope setup or simply differences in manual classification; we have relatively low statistics for this size range. Wang & Palmer[2] make no report on amorphous structures, they excluded unidentifiable atomic structures for their considerations of transformations under the electron beam. An interesting note on the results of Wang & Palmer is that their initial clusters are far from equilibrium distributions, but that under prolonged electron irradiation they reach ratios similar to our study and Wells *et al.*

The distributions of structural isomers in this study of surface grown clusters are a reasonable match to those found in pre-formed clusters deposited after gas condensation and size-selection. Small differences in the distributions of structural isomers could occur because of the formation mechanism, due to counting statistics in this or previous studies, to kinetic trapping of metastable structures in the formation process or to effects of the electron beam.

3. Methods

3.1. Production of nanoclusters

The surface-assembled Au clusters used in this work were prepared by sputtering single atoms from a gold target with an Ar ion beam. First, a Au film is evaporated onto an oxygen-free copper support. Once generated, the film is sputtered with an Ar ion beam (Omicron ISE-5 cold cathode gun) to generate the Au atoms which are soft-landed onto an amorphous carbon-coated TEM grid. In the samples of this study, atoms were deposited with sputtering voltages of 2 and 3 kV.

The size-selected Au clusters used in this work were made by a magnetron sputtering, gas aggregation cluster beam source.[20,21] Clusters are aggregated in rare gas after plasma sputtering of target atoms, accelerated, and focused. The focused beam is then mass-separated by a lateral time-of-flight filter.[22] The clusters are soft-landed onto amorphous carbon-coated copper TEM grids.

3.2. Characterisation using STEM

Images of clusters used to assign structural isomers and to provide calibrated numbers of atoms *versus* diameter were acquired on a probe-corrected JEOL ARM300F (GRAND-ARM) Scanning Transmission Electron Microscope operated at 300 kV at the electron Physical Sciences Imaging Centre (ePSIC) at Diamond Light Source. The probe semi-angle was approximately 23 mrad and the HAADF detector had an inner collection angle of approximately 58 mrad (outer angle approximately 215 mrad).

Sample tilt series were acquired using a probe-corrected Thermo-Scientific Spectra 200 Scanning Transmission Electron Microscope operated at 200 kV at Cardiff University. The probe semi-angle was approximately 30 mrad and the HAADF detector had an inner collection angle of approximately 56 mrad (outer angle approximately 200 mrad).

3.3. Cluster simulations

Idealised cluster structure models were produced in Python using the Atomic Simulation Environment (ASE) package.[23] From these models, HAADF-STEM simulations of clusters were produced, again in Python, using the abTEM package[24] and the multi-slice Plane-wave Reciprocal-Space Interpolated Scattering Matrix (PRISM) algorithm.[25] This method was used to produce both the Simulation Atlas of different cluster sizes and orientations, as well as the hemispherical cluster images used in the tilt series comparison.

The simulations use "magic number" clusters; that is, clusters of a particular number of atoms corresponding to closed shell geometric arrangements of the atoms. These structures are the icosahedron (Ih), decahedron (Dh) and single-crystal fcc (fcc, *i.e.* the bulk-like arrangement). In reality cluster structures deviate from these ideal forms even at magic numbers.

4. Conclusions

We have determined the morphologies of atomic clusters, in the size range 100–1000 atoms, formed by the surface-assembly of Au atoms on amorphous carbon films. The surface grown clusters were found to preferentially form 3-dimensional near-spherical structures over 2-dimensional or hemispherical structures.

The distribution of intensity *vs*. diameter of surface-assembled Au clusters on amorphous carbon films is consistent with quasi-spherical particles. This is further supported by direct observation of tilted clusters, which maintain a circular projected cross-section with an intensity distribution consistent with a quasi-spherical shape.

The distributions of structural isomers in the surface-assembled clusters studied here are largely consistent with those previously reported for clusters formed from a gas-condensation cluster source and deposited onto amorphous carbon. Amorphous clusters dominate the size ranges of 100–228 and 229–435 atoms, which is the major difference we have found in comparison to previous cluster-beam deposition results. Above these sizes, in the range of 436–742 atoms, cluster morphologies begin to be dominated by decahedral and fcc (fcc) structures. A small fraction (12%) of icosahedral structures are observed at cluster sizes below 435 atoms, but this decreases as cluster size increases above this range.

The degree of sphericity and structural isomer distribution found in this study is specific to the Au/C system. The weak interaction between Au and carbon results in limited influence of the support on cluster structure. Systems possessing a strong metal–support interaction will not display the same degree of sphericity due to the influence of support on overall structure.

Data availability

All data used in this paper can be found at **https://doi.org/10.5281/zenodo.11147031**. A Jupyter notebook demonstrating the analysis of intensity data and plotting of Fig. 1 can be found at **https://github.com/TomSlater/Surface-Assembled-Clusters**.

Author contributions

MD was responsible for preparation of the initial report draft. JM made the surface-assembled cluster samples. MD, SL & TJAS were responsible for acquisition, analysis and visualisation of electron microscopy data of clusters for simulation/sample tilting, cluster classification and size/sphericity determination respectively. SL & JM collected classification data and performed the image assignments. REP & TJAS were jointly responsible for the conception, management and coordination of the research activity planning and execution. All authors contributed to the review and editing of the paper.

Conflicts of interest

There are no conflicts to declare.

Acknowledgements

We thank Diamond Light Source for access to and support in use of the electron Physical Science Imaging Centre (TEM Instrument E02, Proposal Number(s): MG28449-6), and gratefully acknowledge EPSRC grant EP/V029797/2 for support of the electron microscopy. We would like to acknowledge the CCI Electron Microscopy Facility which has been part-funded by the European Regional Development Fund through the Welsh European Funding Office, and The Wolfson Foundation. Finally we thank Mr Henry P Hoddinott for the supply of size-selected clusters used as reference materials. The clusters were made using the cluster source located at beamline B07 of Diamond Light Source, which is supervised by Prof. Georg Held.

References

1 D. M. Wells, G. Rossi, R. Ferrando and R. E. Palmer, *Nanoscale*, 2015, **7**, 6498–6503.
2 Z. W. Wang and R. E. Palmer, *Phys. Rev. Lett.*, 2012, **108**, 245502.
3 D. M. Foster, R. Ferrando and R. E. Palmer, *Nat. Commun.*, 2018, **9**, 1323.
4 K. An and G. A. Somorjai, *ChemCatChem*, 2012, **4**, 1512–1524.
5 S. Cao, F. F. Tao, Y. Tang, Y. Li and J. Yu, *Chem. Soc. Rev.*, 2016, **45**, 4747–4765.
6 A. Wang, J. Li and T. Zhang, *Nat. Rev. Chem.*, 2018, **2**, 65–81.
7 B. Roldan Cuenya, *Acc. Chem. Res.*, 2013, **46**, 1682–1691.
8 A. S. K. Hashmi and G. J. Hutchings, *Angew. Chem., Int. Ed.*, 2006, **45**, 7896–7936.
9 F. Baletto, R. Ferrando, A. Fortunelli, F. Montalenti and C. Mottet, *J. Chem. Phys.*, 2002, **116**, 3856–3863.
10 A. S. Barnard, N. P. Young, A. I. Kirkland, M. A. van Huis and H. Xu, *ACS Nano*, 2009, **3**, 1431–1436.
11 S. R. Plant, L. Cao and R. E. Palmer, *J. Am. Chem. Soc.*, 2014, **136**, 7559–7562.
12 K. Koga, T. Ikeshoji and K.-I. Sugawara, *Phys. Rev. Lett.*, 2004, **92**, 115507.
13 Z. Y. Li, N. P. Young, M. Di Vece, S. Palomba, R. E. Palmer, A. L. Bleloch, B. C. Curley, R. L. Johnston, J. Jiang and J. Yuan, *Nature*, 2008, **451**, 46–48.
14 N. P. Young, Z. Y. Li, Y. Chen, S. Palomba, M. D. Vece and R. E. Palmer, *Phys. Rev. Lett.*, 2008, **101**, 246103.
15 T. Risse, S. Shaikhutdinov, N. Nilius, M. Sterrer and H.-J. Freund, *Acc. Chem. Res.*, 2008, **41**, 949–956.
16 S. G. Lambie, G. R. Weal, C. E. Blackmore, R. E. Palmer and A. L. Garden, *Nanoscale Adv.*, 2019, **1**, 2416–2425.
17 I. L. Garzón, K. Michaelian, M. R. Beltrán, A. Posada-Amarillas, P. Ordejón, E. Artacho, D. Sánchez-Portal and J. M. Soler, *Phys. Rev. Lett.*, 1998, **81**, 1600–1603.
18 N. Tarrat, M. Rapacioli and F. Spiegelman, *J. Chem. Phys.*, 2018, **148**, 204308.
19 S. Jindal, S. Chiriki and S. S. Bulusu, *J. Chem. Phys.*, 2017, **146**, 204301.
20 I. M. Goldby, B. von Issendorff, L. Kuipers and R. E. Palmer, *Rev. Sci. Instrum.*, 1997, **68**, 3327–3334.
21 S. Pratontep, S. J. Carroll, C. Xirouchaki, M. Streun and R. E. Palmer, *Rev. Sci. Instrum.*, 2005, **76**, 045103.
22 B. von Issendorff and R. E. Palmer, *Rev. Sci. Instrum.*, 1999, **70**, 4497–4501.
23 A. H. Larsen, J. J. Mortensen, J. Blomqvist, I. E. Castelli, R. Christensen, M. Dułak, J. Friis, M. N. Groves, B. Hammer, C. Hargus, E. D. Hermes, P. C. Jennings, P. B. Jensen, J. Kermode, J. R. Kitchin, E. L. Kolsbjerg, J. Kubal, K. Kaasbjerg, S. Lysgaard, J. B. Maronsson, T. Maxson, T. Olsen, L. Pastewka, A. Peterson, C. Rostgaard, J. Schiøtz, O. Schütt, M. Strange, K. S. Thygesen, T. Vegge, L. Vilhelmsen, M. Walter, Z. Zeng and K. W. Jacobsen, *J. Phys.: Condens. Matter*, 2017, **29**, 273002.
24 J. Madsen and T. Susi, *Open Res. Eur.*, 2021, **1**, 13015.
25 C. Ophus, *Adv. Struct. Chem. Imaging*, 2017, **3**, 1–11.